Neotectonics of the Owen Fracture Zone (NW Indian Ocean): structural evolution of an oceanic strike-slip plate boundary

Mathieu Rodriguez, Marc Fournier, Nicolas Chamot-Rooke, Philippe Huchon, Julien Bourget, M. Sorbier, Sébastien Zaragosi, Alain Rabaute

HAL Id: hal-00643186

https://hal.sorbonne-universite.fr/hal-00643186v1

Submitted on 21 Nov 2011

1   **Neotectonics of the Owen Fracture Zone (NW Indian Ocean): structural evolution of an**

2   **oceanic strike-slip plate boundary**

3   *M. RODRIGUEZ[1,2,3*], M. FOURNIER[1,2], N. CHAMOT-ROOKE[3], P. HUCHON[1,2], J.*

4   *BOURGET[4], M. SORBIER[3], S. ZARAGOSI[4], A. RABAUTE[1,2,3]*

5

6   *(1) Institut des Sciences de la Terre de Paris, UMR 7193, Université Pierre et Marie Curie,*

7   *case 129, 4 place Jussieu, 75252 Paris cedex 05, France*

8   *(2) iSTeP, UMR 7193, CNRS, F-75005 Paris, France*

9   *(3) Laboratoire de Géologie, Ecole normale supérieure, 24 rue Lhomond, 75231 Paris cedex*

10   *05, France*

11   *(4) Université Bordeaux 1, UMR 5805 EPOC, avenue des facultés, 33405 Talence Cedex,*

12   *France*

13

14   **Corresponding author: rodriguez@geologie.ens.fr*

15

16   **Abstract**

17   **The Owen Fracture Zone is a 800 km-long fault system that accommodates the**

18   **dextral strike-slip motion between India and Arabia plates. Because of slow pelagic**

19   **sedimentation rates that preserve the seafloor expression of the fault since the Early**

20   **Pliocene, the fault is clearly observed on bathymetric data. It is made up of a series of**

21   **fault segments separated by releasing and restraining bends, including a major pull-**

22   **apart basin at latitude 20°N. Some distal turbiditic channels from the Indus deep-sea fan**

23   **overlap the fault system and are disturbed by its activity, thus providing landmarks to**

24   **date successive stages of fault activity and structural evolution of the Owen Fracture**

25   **Zone from Pliocene to Present. We determine the durability of relay structures and the**

26   **timing of their evolution along the principal displacement zone, from their inception to**

27   **their extinction. We observe subsidence migration in the 20°N basin, and alternate**

28   **activation of fault splays in the vicinity of the Qalhat seamount. The present-day Owen**

29   **Fracture Zone is the latest stage of structural evolution of the 20-Myr-old strike-slip**

30   **fault system buried under Indus turbiditic deposits whose activity started at the eastern**

31   **foot of the Owen Ridge when the Gulf of Aden opened. The evolution of the Owen**

32   **Fracture Zone since 3-6 Myr reflects a steady state plate motion between Arabia and**

33   **India, such as inferred by kinematics for the last 20 Myr period. The structural**

34   **evolution of the Owen Fracture Zone since 20 Myr– including fault segments**

propagation and migration, pull-apart basin opening and extinction - seems to be characterized by a progressive reorganisation of the fault system, and does not require any major kinematics change.

1. Introduction

Large strike-slip faults in continental or oceanic domains display a variety of geological features that received considerable attention from researchers [*see Mann, 2007 for a synthesis*]. Of particular interest are structures transverse to the main strike-slip fault that take place in areas where the layout of the principal displacement zone is discontinuous or curved. These relay structures accommodate the transfer of slip between adjacent fault segments on both sides of the stepover region. Depending on fault geometry and local stress field, these discontinuities may undergo compression or extension, leading to the formation of a positive relief or a basin, forming a restraining bend or a releasing bend, respectively [*Sylvester, 1988; Cunningham and Mann, 2007*]. Strike-slip stepover regions are often considered as progressively increasing in structural relief (subsidence or uplift) with increasing slip along the principal displacement zone [*Aydin and Nur, 1982; Mann et al., 1983*].

In contrast, recent studies of the San Andreas fault system [*Wakabayashi et al. (2004) and Wakabayashi (2007)*] showed that some stepover regions may migrate along the main strike-slip fault. Further evidence of migration is found in the narrow, elongated Dead Sea pull-apart basin along the Levant fault [*Kashai and Croker, 1987; Ten Brink and Ben Avraham, 1989; Garfunkel and Ben Avraham, 1996; Ten Brink and Rybakov., 1999; Smit et al., 2008*]. In both cases, little structural relieves are generated as compared to what would be expected from the progressive growth model. Basin migration is in contrast to prior observations that, within stepover basins, mature strike-slip systems tend to develop simple through-going faults that accommodate the relative motion [*Zhang et al, 1989*; *Le Pichon et al., 2001; Rangin and Le Pichon, 2004; Ben-Zion and Sammis, 2003; Wesnousky, 2005; Schattner and Weinberger, 2008; Wu et al., 2010; Schattner, 2010; Garcia-Moreno et al., 2010*]. These works thus raise the question of the durability of relay structures and the timing of their evolution along the principal displacement zone, from their inception to their extinction.

We recently surveyed a major strike-slip feature in the Northwest Indian Ocean, which forms the present day India-Arabia plate boundary: the Owen Fracture Zone (OFZ hereafter) [*Matthews, 1966; Whitmarsh et al., 1979; Gordon and DeMets, 1989; Fournier et al., 2008b,*

69   *2011*]. The OFZ is a 800 km-long dextral strike-slip fault which connects the Makran

70   subduction zone to the north and the Aden-Owen-Carlsberg triple junction to the south

71   (Figure 1Figure 1). New bathymetry data collected during the Owen and FanIndien 2009

72   cruises reveal that fault scarps are well preserved on the seafloor and can be followed

73   continuously over hundreds of kilometers, pointing to very active tectonics [*Fournier et al.,*

74   *2011*]. Although the overall geometry of the OFZ follows a small circle about the India-

75   Arabia pole of rotation (i.e. is a pure transform fault), the fault system displays a succession

76   of releasing and restraining bends, with related tectonic features such as the 20°N pull-apart

77   basin (Figure 1Figure 1). South and North, the OFZ terminates into the Beautemps-Beaupré

78   rhomboidal pull-apart basin and the Dalrymple Trough, respectively (Figure 1Figure 1)

79   [*Fournier et al., 2008a, 2011; Edwards et al., 2008*]. The objective of this paper is to

80   constrain the timing of the structural evolution of the OFZ over the Plio-Pleistocene period.

81   Since the OFZ is located at the western end of the Indus turbiditic system, distal turbiditic

82   channels are strongly disturbed by neotectonics of this fault system and provide good

83   landmarks to date the successive stages of fault activation and structural evolution of the

84   OFZ. In some areas, transition from mass transport to pelagic deposition mode can also be

85   related to tectonic events and constrain their dating.

86

87   **2. Tectonic and kinematic setting**

88

89   *2.1. Main structural features of the Owen Fracture Zone and present-day kinematics*

90   The overall shape of the OFZ is curved (Figure 1Figure 1): the fracture zone azimuth

91   increases progressively from N10°E at latitude 15°30'N (Beautemps-Beaupré Basin) to

92   N31°E at the entrance of the Dalrymple Trough at 22°N. The OFZ closely follows a small

93   circle about the rotation pole determined with GPS and seismicity data, which is consistent

94   with a pure strike-slip motion along the entire fracture zone [*Fournier et al., 2011*], in contrast

95   with the increasing transtension north of 18°N predicted by the MORVEL closure-enforced

96   pole [*DeMets et al., 2010*].   The OFZ is made up of six apparently uninterrupted fault

97   segments, ranging in length from 60 to 180 km [*Fournier et al., 2011*]. The fault system is

98   associated with a major morphological feature, the Owen Ridge, which rises up to 2000 m

99   with respect to the surrounding seafloor. The Owen Ridge is disrupted by two morphological

100 thresholds at 18°10'N and 20°N. The entire plate boundary can be divided into five

101 geographic segments, starting from the Beautemps-Beaupré Basin (Figure 1Figure 1): the

102 southern ridge (300 km long), the central ridge (220 km long), the 20° N pull-apart basin

103   (100 km long), the Qalhat seamount, and the Murray Ridge (which is not covered by our

104   dataset). As indicated by dextral strike-slip focal mechanisms of earthquakes along the OFZ

105   (Figure 1) [*Quittmeyer and Kafka, 1984; Gordon and DeMets, 1989; Fournier et al., 2001*],

106   the Arabian plate moves northwards slightly faster than the Indian plate with a relative motion

107   of 3 ±1 mm yr^{-1} estimated independently from geodetic [*Reilinger et al., 2006; Fournier et*

108   *al., 2008b*] and geological [*DeMets et al., 1990, 1994, 2010*] data.

109

110   *2.2. History and origin of the Owen Ridge and the Owen Fracture Zone*

111   Offsets on the seafloor imply a finite dextral displacement of 10-12 km along the OFZ

112   (Figures 2, 3) [*Fournier et al., 2008b, 2011*]. Considering a steady motion of 3±1 mm yr^{-1},

113   this indicates that the present-day trace of the OFZ has been active since 3-6 Myr. The

114   reconstruction of the India-Arabia motion based on magnetic anomalies suggests that the rate

115   of dextral strike-slip motion remained stable along the OFZ since the first stages of seafloor

116   spreading in the Gulf of Aden [*Merkouriev and DeMets, 2006; Chamot-Rooke et al., 2009;*

117   *Fournier et al., 2010*]. This would imply the existence of an at least ~20-Myr-old strike-slip

118   fault system accommodating the Arabia-India motion at the Eastern foot of the Owen Ridge.

119   The trace of the OFZ observed on the seafloor is the latest stage of this strike-slip activity.

120   The southern and central segments of the Owen Ridge were uplifted along this ~20-Myr-old

121   OFZ 19 Myr ago, as attested by the rapid transition from turbiditic to pelagic deposits in

122   DSDP and ODP cores [*Whitmarsh et al, 1974; Shipboard Scientific Party, 1989; Weissel et*

123   *al., 1992*]. [*Patriat et al., 2008*] identify a kinematic change in seafloor spreading on the

124   Southwest Indian Ridge at 24 Ma, and hypothesizes that the collision between Arabia and

125   Eurasia induced a major plate reorganization phase at the scale of the Western Indian Ocean.

126   The uplift and the initiation of seafloor spreading in the Gulf of Aden (dated at 19.7 Myr

127   (Chron 6) [*Whitmarsh, 1979; Fournier et al., 2010*]) most probably occurred in response to

128   this plate reorganization event. The Dalrymple Trough at the northern end of the OFZ is of

129   Early Miocene age too, with an increase in subsidence observed since the Late Miocene

130   [*Edwards et al., 2000; Gaedicke et al., 2002*]. OBS data suggest that the trough developed

131   along a small piece of continental crust, probably inherited from the fragmentation of the

132   Gondwanaland [*Edwards et al., 2000, 2008; Gaedicke et al., 2002*]. At the northern end of the

133   OFZ, the history of the Qalhat Seamount is not clearly established. The nature of the

134   underlying basement remains unknown, as it has never been directly sampled, but the

135   presence of the Little Murray Ridge volcanic seamounts buried under the Oman basin

136   [*Gaedicke et al., 2002; Mouchot, 2009*], coupled with the existence of a strong magnetic

137 anomaly in the vicinity of the seamount and a typical flat top morphology, strongly suggest

138 that the Qalhat Seamount is a volcanic guyot [*Edwards et al., 2000; Fournier et al., 2011*].

139 Onlap of Paleocene sediments onto the Qalhat seamount [*Edwards et al., 2000, 2008;*

140 *Gaedicke et al., 2002*] demonstrates that the seamount is older than Paleocene.

141

142 *2.3. The Owen Ridge and the Indus Fan*

143 The Owen Ridge acts as a topographic barrier for the Indus turbiditic system and

144 isolates the Owen Basin, located west of the Owen Ridge, from any sediment supply from the

145 east [*Whitmarsh, 1979; Mountain and Prell, 1989*]. The Indus turbiditic system covers

146 1.1 x 10^6 km^2, stretching 1500 km into the Indian Ocean from the present delta front [*Clift et*

147 *al., 2001*]. The oldest sediments drilled suggest a Paleogene age for the emplacement of this

148 sedimentary system [*Whitmarsh et al., 1974; Shipboard scientific party, 1989; Weedon and*

149 *McCave, 1991; Qayrum et al., 1997, Ellouz-Zimmermann et al., 2007*]. At its thickest part the

150 fan is more than 9 km thick, but its thickness decreases westward when approaching the

151 Owen and Murray Ridges [*DSDP site 222, Shipboard scientific party, 1972; Clift et al., 2001;*

152 *Calvès, 2008*]. Seismic stratigraphy revealed that channel and levee complexes are most

153 pronounced after the Early Miocene, coincident with a sharp increase in sedimentation rates

154 related to the uplift of the Himalaya [*Clift et al., 2001*]. ODP site 720 located at the southern

155 extremity of the fan documents an alternation of pelagic and short turbiditic episodes over the

156 entire Pleistocene sequence, in response to shifts in the loci of Indus Fan deposition

157 [*Shipboard scientific party, 1989; Govil and Naidu, 2008*].

158

159 **3. Methods and data set**

160 *3.1. Identification of the structure of the Owen Fracture Zone*

161 Bathymetry and acoustic imagery were collected using a Kongsberg-Simrad EM 120

162 echosounder on board the R/V Beautemps-Beaupré operated by the French navy during the

163 Owen and FanIndien 2009 surveys. A DEM at 80 m grid interval was produced as well as

164 mosaics of the acoustic imagery (bottom reflectivity). In addition to bathymetry and

165 reflectivity, the SBP120 sub-bottom profiler coupled with the EM120 provided a set of high

166 frequency (3.5 kHz), high resolution profiles with penetration down to 100 m in fine grained

167 sediments and about 25 m in sand rich floor. Only a AGC has been applied. Because of slow

168 pelagic sedimentation rates along the OFZ since the Early Pliocene [*Shipboard scientific*

169 *party, 1974*], the trace of the fault is well preserved on the seafloor. The fault traces observed

170 on both bathymetric data and SBP120 profiles were mapped. Active faults are expected to be

171 identified by a scarp at the seafloor. However, for some of these faults, it is difficult to assess

172 whether they are active or not. Indeed, in areas dominated by pelagic deposition, the pelagic

173 cover takes the exact shape of the underlying morphology and preserves fault offsets through

174 times. Thus the detection of offsets at the seafloor is not by itself an indicator of the present-

175 day activity of the fault. On the other hand, active faults are well observed in areas dominated

176 by turbiditic processes, since their frequency allows a good record of the progressive offset of

177 growth-faults and associated sedimentary tilting.

178

179 *3.2. Interpretation of sedimentary deposits on SBP120 (3.5 kHz) profiles*

180 We recognize pelagic and turbiditic deposits in the sub-bottom high resolution profiles

181 based on their seismic characters. Where SBP120 profiles display well stratified, continuous

182 and conformable horizons, the deposits are interpreted as pelagic in origin. This interpretation

183 is supported by correlation with DSDP site 222 drill hole (see Figure 1Figure 1 for location),

184 and by the analysis of a Küllenberg core [*Bourget et al., submitted*]. Where SBP120 profiles

185 display well-stratified horizons with successions of high and low amplitude reflections, or

186 thick transparent horizons in pull-apart areas, the deposits are interpreted as turbiditic in

187 origin. This interpretation is also supported by the analysis of a Küllenberg core (Figure 4 for

188 location) [*Bourget et al., submitted*].

189

190 *3.3. Age estimates*

191 Several DSDP and ODP drillings are available in our studied area. Estimated

192 sedimentation rates for the Pliocene pelagic interval are used to date the tectonic and

193 sedimentary events we observe on SBP profiles. All pelagic sedimentation rates estimated at

194 different drilling sites range between ~30 and ~50 m.Myr^{-1} [*Shipboard scientific party, 1974,*

195 *1989*]. There is little spatial variation of Plio-Pleistocene pelagic sedimentation rates along the

196 Owen Ridge, allowing large scale interpolation of these values. In this study, we use

197 sedimentation rates estimated at site DSDP 222, because of its proximity to the OFZ.

198 Sedimentation rates at site DSDP 222 quoted between 43 and 53 m.Myr^{-1} for the last 2 Myr

199 interval [*Shipboard scientific party, 1974*]. Two-way travel time to seismic reflectors was

200 converted to depth using a P-wave velocity of 1500 m.s^{-1}.

201 A different approach based on the analysis of Küllenberg cores is used to estimate the

202 age of turbiditic deposits in the 20°N pull-apart basin. Küllenberg cores were sampled in areas

203 where turbiditic deposits are the thinnest in order to sample the highest number of turbiditic

204 events. The high resolution of SBP 120 profiles allows correlation of turbiditic reflectors with

205   turbiditic deposits identified on Küllenberg cores. Turbiditic deposits are dated using the ^{14}C

206   method on planctonic foraminifera sampled in undisturbed layers of the core. ^{14}C ages

207   obtained for the first turbiditic events are extrapolated to deeper horizons using the constant

208   tilting rate of turbiditic horizons in the 20°N Basin. The method and the role of relative sea

209   level variations in the turbiditic infill of the 20°N Basin are detailed in [*Bourget et al.,*

210   *submitted*].

211

212   **4. Results**

213   In this section, we describe the different segments of the OFZ fault system. We first

214   focus on the dominantly strike-slip portions, and then describe stepover areas. Each

215   description focuses on the geomorphic expression of the OFZ, in relation with the turbiditic

216   channels from the Indus Fan where present. We describe channels whose activity can be used

217   as a time indicator for the relative and/or absolute age of the deformation in stepover areas.

218   The depth of pull-apart basins is given with respect to the surrounding seafloor.

219

220   *4.1. Dominantly strike-slip segments: the south and central Owen Ridge*

221   The southern Owen Ridge consists in a 300 km-long, 50 km-wide, and 2000 m-high,

222   asymmetric relief, with a steep east-facing scarp associated with the OFZ and a gentle western

223   slope dissected by numerous landslides [*Rodriguez et al., submitted*] (**Figure 2**~~Figure 2~~). To

224   the south, the OFZ offsets the southern ridge dextrally over 12 km (Figure 2) [*Fournier et al.,*

225   *2008b*]. The area shows no evidence of vertical motion on the bathymetric data, suggesting

226   dominantly pure strike-slip motion along this segment.

227   Northwards, a minor restraining bend is observed on the Indian plate side at the

228   northern end of the southern ridge (**Figure 2**~~Figure 2~~). The restraining bend corresponds to a

229   series of gentle folds related to the slight deviation of the OFZ trend between 17°N and 18°N.

230   At the same latitude, the vertical throw of the OFZ is maximum. The folds generate a relief up

231   to 120-m-high (**Error! Reference source not found.**~~Figure~~ 2). A similar gentle fold has

232   been observed on ODP seismic profiles [*Shipboard scientific party, 1989*], which appears to

233   have been active during the entire Pleistocene, accommodating about 150 m of vertical

234   motion. Thus a small component of fault-normal compressional motion can be inferred in this

235   area.

236   The central Owen Ridge is a 220-km-long, 50-km-wide, and up to 1700-m-high relief

237   (Figure 3). The central ridge displays an irregular morphology, with a 1300 m-high plateau

238   spreading over 485 km^2 and seamounts dissected by complex networks of gullies and

239 landslides [*Rodriguez et al., submitted*]. The OFZ crosscuts the central ridge between 18°50'N

240 and 19°35'N and offsets it dextrally over 10 km (Figure 3). Southeast of the central ridge (at

241 latitude 18°40'N), a 7-km-wide stepover between two segments of the OFZ gives birth to a

242 releasing bend associated with a small 25-km-long and 90-m-deep pull-apart basin.

243

244 *4.2. The 20°N pull-apart basin releasing bend*

245 The 20°N Basin is 90-km-long and up to 35-km-wide pull-apart basin (**Figure**

246 **4**~~Figure~~ 4). The basin developed in a 12-km-wide stepover between two major strike-slip

247 faults trending N25°E south of the basin and N30°E north of it. The overall structure of the

248 basin is asymmetric, with the OFZ as a steep master fault on the western side, and a single

249 normal fault dividing northwards into several arcuate splays on the eastern side. The throw of

250 arcuate normal faults clusters between 100 m and 300 m, and the associated topographic

251 uplift decreases northwards as the number of faults increases, suggesting partitioning of local

252 extensional deformation. To the southeast of the 20°N basin, a system of en-échelon faults,

253 oriented 25° clockwise with respect to the OFZ is observed between 19°18'N and 19°45'N

254 (Figure 4).

255 The bathymetric map shows three distinct sub-basins (labelled SB1, SB2, and SB3 in

256 **Figure 4**~~Figure~~ 4). SB1 and SB2 extend over 70 km² and 340 km², respectively. SB3 extends

257 over 590 km². E-W-trending transverse normal faults separate the sub-basins. The 20°N basin

258 deepens abruptly northwards, as sub-basins 1, 2, 3 form terraces respectively 60, 100, and

259 360 m deep with respect to the surrounding seafloor (Figure 5). Pelagic deposits blanket SB1

260 and SB2, as well as the half grabens of the eastern hanging wall, whereas recent turbiditic

261 deposits filled in SB3 [*Bourget et al., submitted*]. In SB3, Indus turbiditic deposits adopt

262 vertically a fanning configuration on the longitudinal SBP120 profile (**Figure 5**~~Figure~~ 5).

263 The turbiditic infill forms a subtle and asymmetric syncline on transverse SBP120 profiles

264 (**Figure**~~Figure~~ 6). A change of sense of asymmetry occurs along strike within SB3, where

265 horizons within the southern part of the basin dip toward the west (profile P07b), whereas in

266 the northern section, horizons dip to the east (profile P07a).

267 Although SBP120 profiles do not reach the substratum of the 20°N basin, they give

268 some insights about its deep structure. Turbiditic horizons onlap tilted blocks at the southern

269 end of the 20°N basin (**Figure 5**~~Figure~~ 5). Turbiditic reflectors are slightly disturbed in the

270 northern part of the 20°N basin, as a series of small buried benches, probably related to the

271 activity of a minor normal fault (Figure 5).

272

4.3. Age of the Indus turbiditic channels affected by the opening of the 20°N basin

The opening of the 20°N basin affected the evolution of seven turbiditic channels belonging to three distinct generations labelled A, B, and C in younging order (Figures 5, 7). These channels are located 600 km away from the Indus canyon and are part of the distal Indus fan.

Channel A-generation before the onset of the Owen fracture zone (>3-6 Myr old)

The oldest channel (A1) is located in the Owen Basin and is now disconnected from the Indus fan. This highly meandering channel is now abandoned and covered by a thick (>100 m) pelagic drape (**Figure 4**~~Figures~~ 4, 7). No trace of activity of this channel is observed on SBP120 profiles. Thus, the channel is older than the oldest sub-bottom reflector, the age of which is estimated at 3 Myr based on sedimentation rates at DSDP site 222. It is the minimum age for this channel, which could be older. The presence of channel A1 in the Owen Basin indicates that no significant relief acting as a topographic barrier for sediments coming from the Indus existed during its activity. This channel thus pre-dates the onset of the present-day trace of the OFZ.

The meandering channel A2 is supposed to be of the same generation, since no trace of channel activity is observed on SBP120 data (**Figure** 7). Arcuate normal faults of the 20°N basin crosscut channel A2, the channel being now located on an uplifted area. We thus infer that the uplift post-dates the channel activity.

Other channels (group A3) that do not display any trace of activity at the depth of SBP120 penetration are located in the Indus abyssal plain (**Figure 4**~~Figure~~ 4). This group of channels was subjected to avulsion. As normal faults dissected the bifurcation point, it is difficult to discriminate which channel predates the other. Channel avulsion is known to be an autocyclic process that spans thousands of years [*Babonneau et al., 2002*], but it can be driven by tectonics processes related to the tectonic evolution of the 20°N basin which spans millions years. For that reason, we cannot use the occurrence of avulsion as a tectonic indicator. The channels run parallel to the OFZ and do not seem to have been "attracted" by the presence of any topographic depression during their activity. A normal fault of the 20°N Basin dissects the eastern channel A3. Thus the channel activity seems to pre-date the opening of the basin, and is probably coeval with the channel A1. We infer that the group of channels A3 could be the southward prolongation of channel A2.

Channel B-generation and the opening of the southern sub-basins of the 20°N basin

307   The generation B is composed of three channels. The paleo-activity of these channels is marked by a lens-shaped, rough and chaotic facies on SBP120 profiles (**Figure** 7). Two of them (B1 and B2) are located at the southernmost part of the 20°N basin (**Figure 4**~~Figures~~ 4, 5). The normal fault bounding the southernmost sub-basins 1 and 2 dissects channel B1, which is also incised by the system of en-échelon faults to the east (**Figure 4**~~Figures~~ 4, 8). The complex arcuate normal fault system that borders the eastern side of the 20°N basin strongly dissects channel B3. Small relics of channel B3 are also observed close to the currently active channel on bathymetry. A thick pelagic drape covers lens-shaped features since 1.32 to 0.95 Myr according to sedimentation rates at DSDP site 222.

Channel C-generation and the filling of the present-day 20°N basin

The currently active channel of the 20°N basin (generation C) is recognisable on the seafloor morphology because of its deep incision through the complex normal fault system and its highly meandering sinuosity (**Figure 5**~~Figures~~ 4, 7). It displays a U-shape in cross section. The incision becomes wider at the mouth of the channel. A transparent body is observed on both sides of the channel, and is interpreted as a HARP (high amplitude reflections package) incised by the channel (**Figure** 8). The path of channel C was probably imposed by the growing topography formed by normal faults footwalls.

4.4. Present-day deformation east of the Qalhat Seamount

The northern Owen Ridge, or Qalhat Seamount, is a volcanic guyot that extends between 20°30'N and 22°10'N (**Figure**~~Figure~~ 9). It is a 210-km-long, more than 55-km-wide, and up to 2700-m-high relief, characterized by a flat and 400-m-deep top. It is eroded by complex networks of mass wasting features [*Rodriguez et al., submitted*]. The OFZ runs on the eastern side of the Qalhat Seamount, where it is divided into three major splays. The principal splay (labelled 1 in **Figure**~~Figure~~ 9) trends N 30E° and bends to N20E° at latitude 21°30'N. A second splay (labelled 2 in **Figure**~~Figure~~ 9), located west of the first one, also trends N30E°. Those two splays (1 and 2) delimitate a 160-m-deep, 45-km-long and up to 20-km-wide pull-apart basin. We propose the name of "Qalhat Basin" for this still-unnamed feature. The third splay (labelled 3 in **Figure**~~Figure~~ 9) is composed of an en-échelon fault system, which trends 14° to the east with respect to the main OFZ (splay 1). At latitude 21°35'N, a 700-m-high and arcuate relief interrupts the en-échelon fault system, which merges northwards with the Dalrymple Trough.

The deep structure of this portion of the OFZ has been partly imaged by seismic lines collected by the RSS Charles Darwin (**Figure 3**~~Figure 1~~0) [*Edwards et al., 2000, 2008*]. As suggested by strong magnetic anomalies, seismic lines confirm that an eastward prolongation of the Qalhat Seamount buried under Indus turbiditic deposits underlies the OFZ. Thus, the arcuate relief that disrupts the en-échelon fault system (labelled 3 in **Figure**~~Figure~~ 9) is volcanic in origin. The OFZ forms a flower-structure in this area, with several sub-parallel vertical splays imaged on seismic profile (Figure 10). The currently active fracture zone is one of the several splays of the flower structure.

The Qalhat Basin is the most conspicuous tectonic feature in this area. It displays a needle geometry, with a very elongated depocentre. Arcuate normal faults with vertical throws of 20 to 70 m delimitate two half grabens on the eastern side of the basin. The active OFZ crosses the basin and has accommodated 30 m of vertical slip since its onset, suggesting a negligible extensional component to the strike-slip motion in this area. Complex slope failures are observed on both sides of the Qalhat Basin, which is a catchment for mass transport deposits. Two distinct seismic facies observed on the SBP120 profile that crosses the half graben allow to distinguish two modes of sedimentary deposition in this basin (**Figure 4**~~Figure~~ 11). The transparent and thick body at the bottom is interpreted as the result of mass transport, whereas the covering well-stratified facies is interpreted as pelagic deposits. The currently active depocentre displays a low reflectivity facies, whereas half-grabens display a highly reflective facies (**Figure 5**~~Figure~~ 12). This indicates that the active depocentre is filled in by mass transports deposits from the Qalhat Seamount, whereas the elevated graben is now isolated from such supply and mainly filled in by pelagic deposits, which imprint their signature on seafloor reflectivity.

Two turbiditic channels belonging to the Indus system are of particular interest with regards to the tectonic activity of the OFZ. The first channel (labelled A on **Figure**~~Figure~~ 9) is dissected by an en-échelon fault system. No trace of its activity is observed on SBP120 profiles, suggesting an age older than 3 Myr. The second channel (labelled B on **Figure**~~Figure~~ 9) is dissected by the two splays of the OFZ (labelled 1 and 2 in Figure 10) that border the current depocentre of the Qalhat Basin. The western splay of the OFZ (labelled 2 in **Figure**~~Figure~~ 9) crosscuts some of the meanders of channel B. It indicates that the channel used to pass west of the splay 2. Thus, the channel pre-dates the onset of the OFZ in this area. These turbiditic channels could possibly be coeval with turbiditic channels identified West of the Dalrymple Trough and at the top of the Murray Ridge [*Ellouz et al, 2007; Mouchot, 2009*].

374   Since Indus turbiditic channels on the north-western side of the Dalrymple Trough all
375   pre-date the onset of the trough [*Ellouz et al, 2007; Mouchot, 2009*] and since the turbiditic
376   system of the Makran accretionary wedge does not form any channel [*Bourget, 2009*; *Bourget
377   et al., 2010*], they cannot be used as time indicators for the propagation of the deformation
378   towards the Dalrymple horsetail structure.
379
380   **5. Summary of the constraints on the age of the deformation along the Owen Fracture**
381   **Zone**
382   In this section we discuss the age and relative chronology of deformation along the
383   different segments of the OFZ. In areas where different scenarii are possible, we decipher
384   which one is the most likely in order to propose a detailed history of the structural evolution
385   of the OFZ since the Early Pliocene.
386
387   *5.1. Age of deformation in the restraining bend (southern Owen Ridge)*
388   The fold observed on ODP seismic line [*Shipboard scientific party, 1989*] along the
389   main restraining bend of the southern Owen Ridge offers a good opportunity to follow the
390   deformation rate through time. The fold has been active during the entire Pleistocene. The
391   most recent episode of folding is observed on SBP profile that crosses the restraining bend
392   located between 17°N and 18°N (Figure 3). The restraining bend consists in two folds. A
393   quantitative analysis of the folding rate using sedimentation rates estimated at site ODP 720
394   (32 m.Myr^{-1}) suggests an increase around 0.8 Myr followed by a smooth and constant
395   deformation.
396
397   *5.2. Age of deformation in the vicinity of the 20°N basin*
398   The best chronological record comes from the 20°N pull-apart basin. The onset of the
399   OFZ and the opening of the 20°N basin clearly post-date the activity of channels of the
400   generation A (**Figure 7**~~Figures~~ 4, 7). The first stage of deformation is an uplift associated
401   with normal fault activity. The uplift is recorded at 1.8-1.5 Myr at DSDP site 222, and marks
402   the transition from turbiditic to pelagic deposits [*Shipboard scientific party, 1974*]. This could
403   be a local uplift associated with the local formation of a new fault. However, no trace of
404   channel activity of the B generation is observed either on seafloor bathymetry or on SBP120
405   profiles in the Owen Basin, west to the 20°N Basin. These could be proofs of an incipient
406   20°N basin where channels of the B generation used to discharge turbiditic material. The
407   second stage of extensional deformation corresponds to the development of a series of half

12

408 grabens bounded by the system of en-échelon normal faults between 19°18'N and 19°45'N

409 (**Figure 4**~~Figures~~ 4, 8). The onset of normal faults seems to be responsible of the channel

410 deactivation, as all the channels of the B generation are faulted. Thus, dating the deactivation

411 of channels, i.e. the base of the pelagic blanket that covers lens-shaped features, gives the age

412 of the deformation. If faulting is not responsible of channel deactivation, then faults emplaced

413 latter than the age of the base of the pelagic blanket that covers lens-shaped features, which is

414 therefore the maximal age of faults. The age of the base of the pelagic blanket that seals traces

415 of channel activity is estimated at 1.32 to 0.95 Myr using sedimentation rates calculated at

416 DSDP site 222 (**Figure** ~~Figures~~ 7, 8). Arcuate normal faults on the hanging wall of the 20°N

417 Basin and the en-échelon fault system must be the latter stage of the normal fault system that

418 started to develop at 1.8-1.5 Myr. With regards to the sub-basin SB3, the extrapolation of the

419 ages of turbiditic deposits measured on Küllenberg core samples gives an age of 420 kyr for

420 the deepest sub-bottom reflector imaged (Figure 13) [*Bourget et al., submitted*]. Thus, the

421 sub-basin SB3 is at least 400 kyr old.

422

423   *5.3. Age of deformation in the vicinity of the Qalhat Seamount*

424   All the turbiditic channels in this area pre-date the onset of the present OFZ and the

425 opening of the Qalhat basin (**Figure**~~Figures~~ 9, 14). We could not assess with field evidences

426 the age of the en-échelon fault system labelled "3" in **Figure**~~Figure~~ 9. Field evidences are

427 compatible with two different scenarii. On one hand, the en-échelon fault system could be the

428 very early stage of the present-day OFZ. The alternative is that it is the location of the future

429 OFZ.

430   In the first case (**Figure 14**), the horsetail termination develops in the continuity of the

431 present-day OFZ and not along the en échelon-fault system, suggesting that the formation of

432 the en-échelon fault system predates the formation of the horsetail structure. This scenario is

433 consistent with several analog modelling works [*Aydin and Nur, 1982; Rahe et al., 1998,*

434 *Basile and Brun, 1999; Schlische et al., 2002; Wu et al., 2010*] which show that en-échelon

435 fault systems are usually emplaced at the very early stage of strike-slip deformation. In the

436 second case, the direction of the en-échelon fault system is more consistent with the small-

437 circle predicted for a pure-strike-slip motion than the direction of the present-day OFZ

438 [*Fournier et al., 2011*]. In this latter case, the en-échelon fault system is considered as the

439 incipient stage of the future OFZ. If confirmed, this scenario would lead to a reorganization of

440 the horsetail termination.

The study of the sedimentary infill of the Qalhat Basin can be used to decipher the relative chronology of the deformation in this area. Indeed, the presence of turbiditic or mass transport deposits sealed by a pelagic cover on the graben of the Qalhat Basin (Figure 12) indicates that the graben used to be a part of the Qalhat Basin depocenter, and has been subsequently slightly uplifted (by about 30 m). Thus, the Qalhat Basin used to be wider, and has been restrained by the onset of the currently main arm of the fracture zone which cross-cuts diagonally the basin (FigureFigures 9, 11). We assume that the onset of the diagonal fault is responsible of the graben isolation from mass transport deposits. The age the base of the isolated graben pelagic cover - and thus the age of the Qalhat Basin extinction- occured 0.7 to 0.6 Myr ago assuming pelagic sedimentation rates close to the ones estimated at DSDP site 222 [*Shipboard scientific party, 1974*] (Figures 11, 14).

The uplift observed at the southern end of the Qalhat Basin is likely to post-date the opening of the Qalhat Basin, as the related normal faults are uplifted too. The age of the extinction of the Qalhat Basin is nearly coeval with the onset of the increase in folding observed at the restraining bend along the southern ridge. The uplift could be due to local compression along the OFZ, which could be responsible for the basin extinction too.

5.4. Summary of the history of the Owen Fracture Zone for the last 3-6 Myr

Although the present trace of the OFZ on the seafloor is only 3-6 Myr old, kinematic studies suggest that the relative motion between India and Arabia plates is located along the Owen Ridge since the opening of the Gulf of Aden 20 Myr ago [*Chamot-Rooke et al., 2009; Fournier et al., 2010, 2011*]. Thus the present-day OFZ is the exposed part of a strike-slip corridor which is partly buried under the Indus deep-sea fan. The following chronology focuses on the structural evolution of the exposed part of the OFZ whose activity spans the Plio-Pleistocene period.

1) The Present-day trace of the OFZ emplaced about 3 to 6 Myr ago, as deduced from finite offsets on the seafloor [*Fournier et al., 2011*]. It runs at the foot of the eastern flanks of the southern and the central ridges since this time (Figure 2Figure 2, Figure Figure 3). A horsetail termination (FigureFigure 9) and a rhomboidal pull-apart basin (Figure 2Figure 2) began to develop at the northern and southern ends of the fracture zone, respectively [*Edwards et al., 2000, Fournier et al., 2008a*]. The onset of the horsetail termination could be related to the increase in subsidence of the Dalrymple Trough observed at ~5 Myr by *Gaedicke et al.* [2002].

507   2) 1.8 to 1.5 Myr ago, a tectonic activity possibly related to the first stages of formation of

508   the 20°N Basin is observed on DSDP drilling [*Shipboard scientific party, 1974*].

509   3) An en-échelon fault system and asymmetric transform basins were emplaced 1.3 to

510   0.95 Myr ago at 20°N (**Figure 4**Figures 4, 8, 15).

511   4) A small shortening phase is recorded at the northern extremity of the southern ridge

512   0.8 Myr ago. It could be associated to a slight deviation of the OFZ from its previous

513   trace. It is the last step of a more regional shortening, which started in the Early

514   Pleistocene [*Shipboard scientific party, 1989*].

515   5) It is still unclear when the Qalhat Basin opened, and when the uplift to the south of it

516   occurred. However, it was intersected by the master OFZ fault 0.7 to 0.6 Myr ago

517   (**Figure**Figure 9). The uplift south of the Qalhat Basin could be coeval with the

518   shortening phase identified on the southern ridge.

519   6) Since its opening, the subsidence of the 20°N basin has been relocated in different sub-

520   basins. The currently active sub-basin is at least ~400 kyr old (**Figure 4**Figures 4, 5, 13).

521   Uncertainties remain in the dating exposed above. The age of the en-échelon fault

522   system to the east of the Qalhat Basin, and the age of the uplift south of it, are not assessed by

523   clear field evidences, and the timing of 20°N sub-basins migration needs to be further

524   constrained. This summary must be considered as the most likely relative ages with regards to

525   the general tectonics of the OFZ.

526

527   **6. Discussion**

528   *6.1. Does the structure of the Owen Fracture Zone reflect a steady-state India-Arabia*

529   *relative plate motion?*

530   The structures that we describe above are those formed along a dextral strike-slip

531   boundary since at least 3 Ma. The relative motion between India and Arabia is small (3 ± 1

532   mm/yr), and consequently very sensitive to any change of plate velocities. Indeed, a slight

533   decrease of the northward motion of Arabia would have inverted the motion along the OFZ

534   from dextral to sinistral, which is not observed. We thus conclude that the relative motion has

535   been stable during the Pliocene, which is further supported by the agreement between

536   geodetic and geologic kinematic modelling [*Fournier et al., 2008b; DeMets et al., 2010*]. The

537   finite offset itself (10 to 12 km) is compatible with a constant shear rate during the same

538   period of time (about 3 mm/yr). Taken all together, this confirms that the major structures that

539   we observe along the OFZ, and in particular the pull-apart basins, are younger than 3-6 Myrs.

540   On the other hand, several observations suggest that the dextral strike-slip motion
541   started much earlier, probably when oceanic accretion initiated in the Gulf of Aden. This is
542   supported by kinematics reconstructions [*Chamot-Rooke et al., 2009*] that suggest an
543   initiation of the dextral motion around 17 Ma or slightly earlier, and a finite differential
544   motion between Arabia and India of the order of 80 km. Furthermore, the amount of
545   horizontal extension at both ends of the OFZ seems to be larger than the 10-12 km offsets.
546   Indeed, 10-12 km of offset are not sufficient to create the subsidence calculated at the
547   Beautemps-Beaupré Basin [*Fournier et al., 2008a*]. The Dalrymple Trough itself may have
548   been active as an oblique rifting as early as the Early Miocene, based on stratigraphic studies
549   [*Gaedicke et al., 2002*]. There is thus an apparent mismatch between the present-day active
550   trace of the fault and the inferred age of initiation of strike-slip motion along the Owen Ridge.
551   This consequently raises the question of the location of the OFZ prior to the Pliocene. One
552   possibility is that the old fault system is located in the same area as the present-day fault
553   system, but is buried under Indus turbiditic deposits, as shown by one seismic profile across
554   the northern OFZ (**Figure 10**). This profile clearly shows more splays than active fault traces
555   at the surface. Acceleration of the turbiditic sedimentation rate between 15 Ma and 5 Ma
556   [*Shipboard scientific party, 1974, 1989; Clift et al., 2001*], in relation with the uplift of the
557   Tibet and the correlative increase in the erosional rates, may have favored such a burial.
558   Considering that the trace of the fault system on seafloor morphology is the result of the
559   competition between the fault activity and sedimentation rates, the presence of the turbiditic
560   channel A1 in the Owen Basin can be explained by a period where sedimentation rates were
561   high enough to entirely cover the active trace of the OFZ fault system.
562   The initiation of the present-day fault trace is synchronous with an increase of the
563   subsidence rate in the Dalrymple Trough and the uplift of the Murray Ridge around 4-5 Myrs
564   [*Gaedicke et al., 2002*]. However, this Pliocene change does not correlate with any known
565   plate-scale regional kinematic changes or major regional tectonic events [*Lepvrier et al.,*
566   *2002; Delescluse and Chamot-Rooke, 2007; Fournier et al., 2004, 2006, 2011*]. Therefore,
567   the structural evolution of the OFZ since 20 Myr and the onset of the present-day trace of the
568   OFZ 3-6 Myr ago both fit into the scheme of a continuum of deformation and a gradual
569   reorganization of the OFZ unrelated to any major kinematics change.
570
571   *6.2. Main characteristics of the structural evolution of the Owen Fracture Zone*
572   In this section, we emphasize the main characteristics of the last structural
573   reorganization of the OFZ since 3-6 Myr through a comparison with other transform plate

16

574 boundaries, mainly the Levant Fault [*Aydin and Nur, 1982; TenBrink and Ben Avraham,*
575 *1989; Lazar et al., 2006*], the San Andreas Fault [*Wakabayashi et al., 2004; Wakabayashi,*
576 *2007*], and a large continental strike-slip fault: the Hayuan fault in China [*Zhang et al., 1989*].
577
578 *6.2.1. Role of structural inheritance in the structural evolution of the Owen Fracture*
579 *Zone*
580 Several observations suggest a control of structural inheritance in the reorganization of
581 the OFZ fault system. First, the topographic relief of the Owen Ridge does not seem to affect
582 the location of the OFZ, which runs alternatively across the slope or at the eastern foot of the
583 Owen Ridge (Figures 2, 3). This conspicuous configuration could be the result of the
584 reactivation of a buried splay of the OFZ. Secondly, the activation of the 0.7-0.6 Myr old
585 segment of the OFZ in the area of the Qalhat Basin could be the result of the reactivation of a
586 buried splay of the flower structure identified in this area (**Figure**Figures 9, 10, 14). Basin
587 inception and extinction thus seem to be related to the alternate activation of fault segments in
588 the fracture zone. This situation is very similar to the one observed at the Dayinshui Basin
589 located along the Haiyuan Fault in China [*Zhang et al., 1989*]. Even if the OFZ
590 accommodated only 10-12 km of relative motion [*Fournier et al., 2011*], the structural
591 evolution of the OFZ in the area of the Qalhat Basin could possibly show a transition from a
592 diffuse to a more localized deformation pattern with increasing maturity of strike-slip motion,
593 as observed elsewhere [*Le Pichon et al., 2001; Ben-Zion and Sammis, 2003; Wesnousky,*
594 *2005; Schattner and Weinberger, 2007; Wu et al., 2010; Garcia-Moreno et al., 2010*]. The
595 deformation tends to localize on pre-existing major fault segments with time.
596
597 *6.2.2. Asymmetry and inception of pull-apart basins along the Owen Fracture Zone*
598 All pull-apart basins developped along the OFZ are asymmetric (18°40'N, 20°N,
599 Qalhat Basin). Asymmetric basins are commonly observed along strike-slip faults [*Ben*
600 *Avraham and Zoback, 1992; Brothers et al., 2009; Seeber, 2010*] and interpreted as the result
601 of transform normal extension. Asymmetry exists even at the scale of the sub-basin SB3 of
602 the 20°N Basin (**Figure**Figure 6), which compares closely with the Zofar Basin along the
603 Levant fault because of the reversal of its asymmetry [*Frieslander, 2000*].
604 The activity of pull-apart basins along the OFZ spans over different time-scales. The
605 opening of pull-apart basins at 20°N 1.8 to 1.5 Myr ago is not coeval with the activation of the
606 present-day OFZ 3-6 Myr ago. (**Figure 7**Figure 15). When the main releasing bend formed at
607 20°N 1.8 to 1.5 Myr ago, the OFZ was already emplaced since 20 Myr. This is similar to the

608   timing of emplacement of the Dead Sea Basin 3 to 5 Myr ago along the 17 to 11.5 Myr old

609   Levant Fault [*Le Pichon and Gaulier, 1988; Garkunkel and Ben Avraham, 2001*] in response

610   to a small gradual change in relative plate kinematics [*Garfunkel, 1981*]. It may also be

611   compared to the emplacement of the Olema Creek formation 110 to 185 kyr ago along the 18

612   Myr old San Andreas Fault [*Wakabayashi et al., 2007*].

613

614   *6.2.3. Migrating subsidence along the Owen Fracture Zone*

615   Several observations suggest that subsidence migration is one of the main

616   characteristic of the OFZ fault system reorganisation since 3-6 Myr. The 20°N basin displays

617   a series of three sub-basins (**Figure 4**~~Figure~~ 4). Sub-basin 2 is 40 m deeper than sub-basin 1,

618   and sub-basin 3 is 260 m deeper than sub-basin 2. Sub-basins 1 and 2 were topographically

619   isolated from the turbiditic supply of the currently active channel since its inception in this

620   area and are sealed by a pelagic blanket. The topography of sub-basins 1 and 2 is flat, whereas

621   the topography of sub-basin 3 is gently tilted, so as the corresponding turbiditic layers

622   (**Figure 5**~~Figure~~ 5). These observations indicate that subsidence is currently inactive in sub-

623   basin 1 and 2, and is localized in sub-basin 3. Subsidence initiated to the south of the 20°N

624   Basin, and migrated northwards, creating deeper and younger sub-basins bounded by

625   transverse faults.

626   This situation is very close to what is observed in the case of the Dead Sea pull-apart

627   basin [*Aydin and Nur, 1982; TenBrink and Ben Avraham, 1989; Lazar et al., 2006*] and the

628   San Andreas Fault system [*Wakabayashi et al., 2004; Wakabayashi, 2007*] where episodes of

629   migration of subsidence are documented [*Kashai and Croker, 1987; Garfunkel and Ben*

630   *Avraham, 1996*]. The active Dead Sea Basin is indeed divided in two sub-basins separated by

631   a transverse fault, the northern one being 350 m deeper than the southern one. However,

632   subsidence migration in the Dead Sea is still a matter of debate, and alternate interpretations

633   have been proposed [*Ben Avraham and Schubert, 2006, Lazar et al., 2006 and Ben Avraham*

634   *et al., 2008*].

635   Sandbox laboratory experiments performed by [*Smit et al., 2008*] show that migration

636   of sub-basins occurs where the ratio between the strike-slip faults spacing and the thickness of

637   the deforming layer is <1. [*Smit et al., 2008*] conclude that this ratio determines not only the

638   basin width, but also its geometry and the migration of subsidence. In these models simulating

639   the migration of subsidence, the intrabasinal transverse faults appear during basin migration,

640   and do not result from the reactivation of previous faults dividing the basin, consistently with

641   observations of [*Kashai and Croker, 1987*] on the Dead Sea Basin.

642   In the case of the 20°N Basin, the subsidence migrated much faster than the

643 displacement accommodated along the OFZ during the last million years (more than 60 km of

644 displacement for the depocenter, versus less than 10 km of displacement along the master

645 fault). Following the nomenclature proposed by [*Wakabayashi et al., 2007*], sub-basins SB1

646 and SB2 are interpreted as the "wake" of the active depocenter (**Figure 4**~~Figure~~ 4). In the

647 light of the model of [*Smit et al., 2008*], the active transverse syn-subsidence faults observed

648 in the active sub-basin 3 (**Figure 5**~~Figure~~ 5) could be incipient stages of future transverse

649 faults that isolate and concentrate the subsidence. If verified, this would confirm the tendency

650 of subsidence to localize in a smaller but deeper sub-basin, without increasing the overall size

651 of the releasing bend with increasing offset along the master fault.

652

653 **7. Conclusions and perspectives**

654   The present day India-Arabia plate boundary emplaced at the location of the OFZ 3 to

655 6 Myr ago. The structural evolution of the OFZ was principally marked by the development

656 of a major releasing bend at 20°N ~1.8-1.5 Myr ago and subsequent subsidence migration,

657 local compression at 17°30'N and 20°30'N ~0.8 Myr ago, and the extinction of the Qalhat

658 Basin 0.7 Myr ago. The structural evolution of the OFZ since the Pliocene suggests a

659 continuous adjustment to a steady-state relative plate motion between the Arabian and Indian

660 plates. The present day OFZ strike-slip system is the latest stage of evolution the India-Arabia

661 plate boundary. Older stages of evolution need to be further constrained by deeper seismic

662 lines. Indeed, the structure of the inferred 20-Myr-old buried strike-slip system that

663 accommodated the motion between India and Arabia since the opening of the Gulf of Aden

664 has not been clearly observed. The location of the India-Arabia plate boundary for the

665 Paleogene-Early Miocene interval is far less known. Kinematics modelling [*Royer et al.,*

666 *2002*] and geological studies [*Edwards et al., 2000*] postulate that the OFZ was located in the

667 Owen Basin at those times, but there is no structural evidence for this hypothesis.

668

676 comments. We thank Baptiste Mulot, Pierpaolo Dubernet and Matthias Delescluse for their

677 technical assistance. We acknowledge the support of SHOM, IFREMER, CEA (LRC Yves-

678 Rocard) and INSU-CNRS for the Owen and the Fanindien 2009 cruises and their support of

679 M. Rodriguez thesis.

680

681 **Figure captions**

682

683 Figure 1. Multibeam bathymetric map of the Owen Fracture Zone acquired during the Owen

684 and Fanindien cruises, with location of figures 2 to 5. Shallow seismicity since 1973 (focal

685 depth < 50 km, magnitude > 2), from USGS/NEIC database (yellow dots), Engdhal et al.

686 (1998, white dots), CMT Harvard database (red dots), and Quittmeyer and Kafka (1984; green

687 dots), and earthquake focal mechanisms for the Owen fracture zone. The seismicity along the

688 OFZ is moderate, the maximum magnitude recorded to date being a Mw 5.8 earthquake.

689 However infrequent but large earthquake may be expected as at other slow boundaries. Inset

690 shows the regional tectonic setting of the India-Arabia plate boundary. AOC: Aden-Owen-

691 Carlsberg triple junction, B^3: Beautemps-Beaupré basin, ITS: Indus turbiditic system, OFZ:

692 Owen fracture zone, Sh: Sheba Ridge.

693

694 Figure 2. a) Slope gradient map of the OFZ along the southern Owen Ridge. b) Inset shows

695 the restraining bend which initiates where the trend of the linear segment of the OFZ slightly

696 deviates and divides into two splays. The inactive splay is buried under mass transport

697 deposits from the southern ridge. The maximal vertical throw of the OFZ is associated to the

698 maximal vertical throw of the restraining bend. **c)** 3.5 kHz profile running through the

699 restraining bend (see inset b) for location). A slight and abrupt increase in folding is observed

700 at ~0.8 Myr (see text).

701

702 Figure 3. Slope gradient map of the OFZ along the central Owen Ridge. A pull-apart basin is

703 observed at 18°40'N. The OFZ offset dextrally the Owen Ridge over 10 km.

704

705 Figure 4. Slope gradient map of the asymmetric 20°N pull-apart basin, and interpretative

706 structural scheme. SB: Sub-basin. A, B, C: channels. Inset shows the en-échelon fault system

707 located to the south east.

708
709

710   Figure 5. a) topography of the 20°N Basin. SB1 and SB2 are flat, whereas SB3 is gently

711   tilted. 3.5 kHz profiles oriented longitudinally along the 20°N basin b) across the inactive sub-

712   basin SB1 and SB2; and c) across the active sub-basin SB3 (see Figure 4Figure 4 for

713   location). Major transverse faults are observed at the seafloor (Figure 4Figure 4) whereas

714   minor transverse faults show only on SBP120 profiles since vertical deformation is erased by

715   rapid deposition. The pelagic blanket of SB1 and SB2 was gently and progressively folded by

716   flexural deformation.

717

718   Figure 6. 3.5 kHz profiles oriented transverse to the 20°N basin (see Figure 4Figure 4 for

719   location). The profile a) runs across the sub-basin SB3 and the DSDP 222 site, allowing

720   correlations of the ages deduced from sedimentation rates. The profile b) runs across sub-

721   basin SB3. c) zoom of profile a) showing the location of DSDP site 222 and the picking of the

722   pelagic reflector that seals the activity of turbiditic channel B3. The pelagic drape is imaged

723   by conformable reflectors and is composed of detrital clay nanno-ooze to nanno-rich detrital

724   carbonate silty clay [DSDP site 222, *Shipboard scientific party, 1974*]. The trace of activity of

725   the turbiditic channel is imaged by a chaotic and rough facies. The age of 0.95 - 1.32 Myr is

726   deduced from pelagic sedimentation rates calculated at site DSDP 222.

727

728   Figure 7. 3.5 kHz profiles across the turbiditic channels affected by the opening of the 20°N

729   basin (see Figure 4Figure 4 for location). Channel activity is imaged by a rough and chaotic

730   facies on SBP profile.

731

732   Figure 8. 3.5 kHz profile across the "en-échelon" fault system located at the southern end of

733   the 20°N basin (see Figure 4Figure 4 for location). The sedimentary filling that onlaps tilted

734   blocks must be the result of fast deposition related to channel B2, as it lies between two

735   concordant layers of pelagic deposits on the southern part of the SBP profile. It is therefore

736   interpreted as mixed turbiditic and pelagic deposits.

737

738   Figure 9. Slope gradient map of the OFZ along the Qalhat Seamount, and interpretative

739   structural scheme. 1, 2, 3: splays of the OFZ; A, B: channels. Inset shows a turbiditic channel

740   dissected by the splays of the OFZ. A part of the slope gradient map is derived from data

741   published in [*Bourget et al., 2009*].

742

Figure 310. Seismic profile modified from Edwards et al. (2000), showing a negative flower structure buried under turbiditic deposits at the eastern foot of the Qalhat Seamount (see FigureFigure 9 for location).

Figure 411. 3.5 kHz profile across the elevated graben of the Qalhat Basin (see FigureFigure 9 and Figure 5Figure 12 for location). Mass Transport Deposits (MTD) are observed beneath the pelagic cover. The graben used to be a catchment for MTD but it is now isolated because of the onset of the main OFZ that crosscuts the Qalhat Basin.

Figure 512. Reflectivity map of the Qalhat Basin (see FigureFigure 9 for location). The low reflectivity area indicates that the present-day depocenter is still a catchment for Mass Transport Deposits (MTD), whereas the high reflectivity facies of the graben indicates that it is not supplied by MTDs anymore.

Figure 13. A) Blow-up of 3.5 kHz profile 2 (see figure 5) showing the location of the site of tilt measurement. The first ten meters have been sampled by Küllenberg cores. B) Relation between the tilt of turbiditic deposits and their age. The tilt of turbiditic horizons in sub-basin 3 is measured on SBP profiles (see Figure 5Figure 5 for location) and corrected from vertical exaggeration ^{14}C ages are available for turbiditic events 1 to 8 [*Bourget et al., submitted*]. The relation between the tilt of turbiditic horizons and ^{14}C ages is fairly linear, suggesting a constant rate of tilting through times. C) The measurement of the tilt of turbiditic horizons can be used as a time indicator for deeper horizons unsampled by küllenberg cores according to the relation obtained in Figure B. The deepest turbiditic deposit we could date is 420 kyr old.

Figure 614. Chronology of the evolution of the Owen fracture zone (OFZ) in the vicinity of the Qalhat Seamount. Stages are younger from a) to d), although they cannot be precisely dated. Figure 16 shows the structural evolution of the OFZ in the case where the en-échelon fault system pre-dates the onset of the horsetail termination. The identification of mass transport deposits (MTD) on the 3.5 kHz profile of figure 12 indicates that the Qalhat Basin used to be wider (stage c) before being crosscut by the present-day main OFZ 0.8 to 0.7 Myr ago (stage d) An alternative interpretation is that the en-échelon fault system developed recently and could be the incipient future OFZ.

Figure 715. Chronology of the opening and the evolution of the 20°N basin.

777 a) Schematic reconstruction of the OFZ at 20°N before 3 Myr. Channels of the generation A

778 are active. The location of channel A1 west of the OFZ could indicate that the active trace of

779 the fault system was probably buried under turbiditic deposits at those times. b) Schematic

780 reconstruction of the OFZ at 20°N at 1.8-1.5 Myr. Transition of sedimentary facies recorded

781 at DSDP site 222 indicates fault activity at those times, which could be related to incipient

782 stages of formation of the 20°N pull-apart basin. Turbiditic channels of generation B were

783 probably active and could have canalized turbiditic deposits to the incipient 20°N Basin. c)

784 Schematic reconstruction of the OFZ at 20°N at 1.32-0.95 Myr. Turbiditic channels of the

785 generation B are inactive, probably because of the opening of the 20°N Basin. The active

786 depocenter was wider than it is today. d) Schematic reconstruction of the OFZ at 20°N since

787 at least 400 kyr. Between 1.32-0.95 Myr and 400 kyr, the 20 °N Basin has undergone

788 subsidence delocalization in the smaller but deeper sub-basin 3. Turbiditic channel C

789 activated and filled in the sub-basin 3.

790

791

792

793 **References**

794 Aydin, A. and A. Nur (1982), Evolution of pull-apart basins and their scale independence,
795   *Tectonics*, *1*, 91-105, doi:1029/TC001i001p00091.

796 Babonneau, N., B. Savoye, M. Cremer, and B. Klein **(**2002), Morphology and architecture of
797   the present canyon and channel system of the Zaire deep-sea fan, *Mar. Pet. Geol.*, *19*, 445-
798   467.

799 Basile, C. and J.P. Brun (1999), Transtensional faulting patterns ranging from pull-apart
800   basins to transform continental margins: an experimental investigation, *J. Struct. Geol.*, *21*,
801   23–37.

802 Ben-Avraham, Z. and M.D. Zoback (1992), Transform normal extension and Asymmetric
803   basins: an alternative to pull-apart models, *Geology*, *20*, 423–426.

804 Ben Avraham Z and G. Schubert (2006), Deep "drop down "basin in the southern Dead Sea,
805   *Earth Planet. Sci. Lett.*, *251*, 254-63.

806 Ben Avraham Z., Z. Garfunkel, M. Lazar (2008), Geology and evolution of the southern Dead
807   Sea Fault with emphasis on subsurface structure, *Annu. Rev. Earth Planet. Sci.*, *36*, 357-87

808 Bourget, J. (2009) Les systèmes turbiditiques du golfe d'Oman et de la marge Est-africaine:
809   architecture, évolution des apports au quaternaire terminal, et impact de la distribution
810   sédimentaire sur les propriétés géoacoustiques des fonds, PhD thesis, 404 pp., Univ.
811   Bordeaux 1, France.

812 Bourget, J., S. Zaragosi, T. Mulder, J.-L. Schneider, T. Garlan, A. Van Toer, V. Mas, N.
813   Ellouz-Zimmermann (2010), Hyperpycnal-fed turbidite lobe architecture and recent
814   sedimentaryprocesses: A case study, *Sediment. Geol. 229*, 144-159
815   doi:10.1016/j.sedgeo.2009.03.009

816 Bourget, J., S. Zaragosi, N. Ellouz-Zimermann, N. Mouchot, T. Garlan, J-L Schneider, V.
817   Lanfumey, S. Lallemant (2010), Turbidite system architecture and sedimentary processes
818   along topographically complex slopes: the Makran convergent margin, *Sedimentology, 58,*
819   376-406, doi: 10.1111/j.1365-3091.2010.01168.

820 Bourget, J., S. Zaragosi, M. Rodriguez, M. Fournier, T. Garlan, N. Chamot-Rooke, Late
821   Quaternary megaturbidites of the Indus Fan: origin and stratigraphic significance.
822   *Submitted to Marine Geology*.

823

824

825 Brothers, D.S., N.W. Driscoll, G.M. Kent, A.J. Harding, J.M. Babcock, R.L. Baskin (2009),

826   Tectonic evolution of the Salton Sea inferred from seismic reflection data, *Nature*

827   *Geoscience*, *2*, 581-584, doi: 10.1038/ngeo590.

828 Calvès, G. (2008), Tectonostratigraphic and climatic record of the NE Arabian Sea, PhD

829   thesis, 305 pp., Univ. Aberdeen, U.K.

830 Chamot-Rooke, N., M. Fournier, Scientific Team of AOC and OWEN cruises (2009),

831   Tracking Arabia-India motion from Miocene to Present, American Geophysical Union,

832   Fall Meeting 2009.

833 Clift, P. D., N. Shimizu, G. D. Layne, J. S. Blusztain, C. Gaedicke, H. U. Schluter, M. K.

834   Clark, and S. Amjad (2001), Development of the Indus Fan and its significance for the

835   erosional history of the Western Himalaya and Karakoram, *Geol. Soc. Am. Bull.*, *113*,

836   1039-1051.

837 Cunningham, W. D. and P. Mann, (2007), Tectonics of strike-slip restraining and releasing

838   bends, in *Tectonics of Strike-Slip Restraining and Releasing Bends*, edited by W.D.

839   Cunningham and P. Mann, *Geol. Soc. Spec. Publ.*, *290*, 1–12.

840 Delescluse, M. and N. Chamot-Rooke (2007), Instantaneous deformation and kinematics of

841   the India-Australia Plate, *Geophys. J. Int.*, *168*, 818-842, doi: 10.1111/j.1365-

842   246X.2006.03181.x

843 DeMets, C., R.G. Gordon, D.F. Argus and S. Stein (1990), Current plate motions, *Geophys. J.*

844   *Int.*, *101*, 425-478.

845 DeMets, C., R.G. Gordon, D.F. Argus and S. Stein (1994), Effect of recent revisions of the

846   geomagnetic reversal time scale on estimates of current plate motions, *Geophys. Res. Lett.*

847   *21*, 2191-2194

848 DeMets C., R. G. Gordon and D.F. Argus (2010), Geologically current plate motions,

849   *Geophys. J. Int., 181,* 1-80, doi: 10.1111/j.1365-246X.2009.04491.x,.

850 Edwards R.A., T. A. Minshull and R. S. White (2000), Extension across the Indian–Arabian

851   plate boundary: the Murray Ridge, *Geophys. J. Int.*, *142*, 461-477.

852 Edwards, R. A., T. A. Minshull, E. R. Flueh and C. Kopp (2008), Dalrymple Trough: An

853   active oblique-slip ocean-continent boundary in the northwest Indian Ocean, *Earth Planet.*

854   *Sci. Lett.*, *272*, 437-445.

855 Ellouz Zimmermann, N. et al. (2007b), Offshore frontal part of the Makran accretionary

856   prism (Pakistan) the Chamak Survey, in *Thrust Belts and Foreland Basins: From Fold*

857   *Kinematics to Hydrocarbon Systems*, edited by O. L. Lacombe et al., pp. 349–364,

858   Springer, Berlin.

859   Engdahl, E.R., R. van der Hilst and R. Buland (1998), Global teleseismic earthquake
860   relocation with improved travel times and procedures for depth determination, *Bull. Seism.*
861   *Soc.Am.*, *88*, 722-743.

862   Fournier, M., N. Bellahsen, O. Fabbri, and Y. Gunnell (2004), Oblique rifting and
863   segmentation of the NE Gulf of Aden passive margin, *Geochem. Geophys. Geosyst., 5,*
864   Q11005, doi:10.1029/2004GC000731.

865   Fournier, M., C. Lepvrier, P. Razin and L. Jolivet (2006), Late Cretaceous to Paleogene post-
866   obduction extension and subsequent Neogene compression in the Oman Mountains,
867   *GeoArabia, 11,* 17-40.

868   Fournier, M., C. Petit, N. Chamot-Rooke, O. Fabbri, P. Huchon, B. Maillot, and C. Lepvrier
869   (2008a), Do ridge-ridge-fault triple junctions exist on Earth? Evidence from the Aden-
870   Owen-Carlsberg junction in the NW Indian Ocean, *Basin Research*, *20*, 575-590, doi:
871   10.1111/j.1365-2117.2008.00356.x

872   Fournier, M., N. Chamot-Rooke, C. Petit, O. Fabbri, P. Huchon, B. Maillot, and C. Lepvrier
873   (2008b), In-situ evidence for dextral active motion at the Arabia-India plate boundary,
874   *Nature Geoscience, 1*, 54-58, doi:10.1038/ngeo.2007.24.

875   Fournier, M., N. Chamot-Rooke, C. Petit, P. Huchon, A. Al-Kathiri, L. Audin, M.-O. Beslier,
876   E. d'Acremont, O. Fabbri, J.-M. Fleury, K. Khanbari, C. Lepvrier, S. Leroy, B. Maillot,
877   and S. Merkouriev (2010), Arabia-Somalia plate kinematics, evolution of the Aden-Owen-
878   Carlsberg triple junction, and opening of the Gulf of Aden, *J. Geophys. Res., 115*, B04102,
879   doi:10.1029/2008JB006257.

880   Fournier, M., N. Chamot-Rooke, M. Rodriguez, P. Huchon, C. Petit, M.-O. Beslier, and S.
881   Zaragosi (2011), Owen Fracture Zone: the Arabia-India plate boundary unveiled*, Earth*
882   *Planet. Sci. Lett., 302,* 247-252, doi:10.1016/j.epsl.2010.12.027.

883   Fournier, M., P. Patriat and S. Leroy (2001), Reappraisal of the Arabia-India-Somalia triple
884   junction kinematics, *Earth Planet. Sci. Lett., 189*, 103-114.

885   Frieslander, U. (2000), The structure of the Dead Sea transform emphasizing the Arava using
886   new geophysical data, Ph.D. thesis, 204 pp., Hebrew University of Jerusalem, Israel.

887   Gaedicke, C., A. Prexl, H.U. Schlüter, H. Roeser and P. Clift (2002), Seismic stratigraphy and
888   correlation of major regional unconformities in the northern Arabia Sea, in *The Tectonic*
889   *and Climatic Evolution of the Arabian Sea Region*, edited by P. Clift, D. Kroon, C.
890   Gaedicke and J. Craig, *Geol. Soc. Spec. Publ.*, *195*, 25-36.

891   Garcia Moreno, D., A. Hubert Ferrari, J. Moernaut, J.G. Fraser, X. Boes, M. Van Daele, U.
892   Avsar, N. Cagatay and M. De Batist (2010), Structure and recent evolution of the Hazar

893   Basin: a strike slip basin on the East Anatolian Fault, Eastern Turkey, *Basin Research*, *23*,
894   191-207, doi: 10.1111/j.1365-2117.2010.00476.

895 Garfunkel, Z. (1981), Internal structure of the Dead Sea leaky transform (Rift) in relation to
896   plate kinematics, *Tectonophysics*, *80*, 81-108.

897 Garfunkel, Z. and Z. Ben-Avraham (1996), The structure of the Dead Sea basin,
898   *Tectonophysics*, *266*, 155–176.

899 Garfunkel, Z. and Z. Ben-Avraham (2001), Basins along the Dead Sea transform, in *Peri-*
900   *Tethys Memoir 6: Peri-Tethyan Rift/Wrench Basins and Passive Margins*, edited by P.A.
901   Ziegler, W. Cavazza, A.H.F. Robertson, and S. Crasquin-Soleau, Mémoires Museum
902   National d'Histoire Naturelle de Paris, 186, 607–627.

903 Gordon, R.G. and C. DeMets (1989), Present-day motion along the Owen fracture zone and
904   Dalrymple trough in the Arabian Sea. J. Geophys. Res. 94, 5560-5570.

905 Govil, P. and P. D. Naidu (2008), Late Quaternary changes in depositional processes along
906   the western margin of the Indus Fan, *Geo-Marine Letters*, 28**,** 1-6.

907 Kashai, EL. and P. F. Croker (1987), Structural geometry and evolution of the Dead Sea-
908   Jordan rift system as deduced from new subsurface data, *Tectonophysics*, *141*, 33-60.

909 Lazar, M., Z. Ben-Avraham and U. Schattner (2006), Formation of sequential basins along a
910   strike-slip fault - geophysical observations from the Dead Sea basin, *Tectonophysics*, *421*,
911   53–69.

912 Le Pichon X., and J.M. Gaulier (1988), The rotation of Arabia and the Levant fault system,
913   *Tectonophysics*, *153*, 271-94

914 Le Pichon X., A.M.C. Sengor, E. Demirbag, C. Rangin, C. Imren, R. Armijo, N. Gorue, N.
915   Cagatay, B. Mercier de Lepinay, B. Meyer, R. Saatcilar and B. Tok (2001), The active
916   main Marmara fault, *Earth Planet. Sci. Lett*., *192*, 595 – 616.

917 Lepvrier, C., M. Fournier, T. Bérard, and J. Roger (2002), Cenozoic extension in coastal
918   Dhofar (southern Oman): Implications on the oblique rifting of the Gulf of Aden,
919   *Tectonophysics, 357,* 279-293.

920 Mann, P., M. R. Hempton, D.C. Badley, and K. Burke (1983), Development of pull-apart
921   basins, *Journal of Geology*, *91*, 529–554.

922 Mann, P. (2007), Global catalogue, classification and tectonic origins of restraining- and
923   releasing bends on active and ancient strike-slip fault systems, *Geol. Soc. Spec. Publ*., *290*,
924   13-142.

925 Matthews D. H. (1966), The Owen Fracture Zone and the northern end of the Carlsberg
926   Ridge, *Phil. Trans. Royal Soc*., A, *259*, 172-186.

927 Menesguen C. (2010), Etude du remplissage et de l'évolution d'un bassin pull-apart le long de
928   la Zone de Fracture d'Owen. Master thesis, 37 pp., Univ. Bordeaux 1, France.

929 Merkouriev, S. and C. DeMets (2006), Constraints on Indian plate motion since 20 Ma from
930   dense Russian magnetic data: Implications for Indian plate dynamics, *Geochem. Geophys.*
931   *Geosyst.*, 7, Q02002, doi:10.1029/2005GC001079.

932 Mouchot, N. (2009), Tectonique et sédimentation sur le complexe de subduction du Makran
933   pakistanais. PhD thesis, 364 pp., Univ. Cergy-Pontoise, France.

934 Mountain, G.S. and W. L. Prell (1989), Geophysical Reconnaissance Survey for ODP Leg
935   117 in the Northwest Indian Ocean, in *Proc. ODP, Init. Repts., Leg 117*, edited by W.L.
936   Prell and N. Niitsuma, 117, pp. 51-64, College Station, TX.

937 Patriat, P., H. Sloan and D. Sauter (2008), From slow to ultraslow : a previously undetected
938   event at the Soutwest Indian Ridge at ca. 24 Ma, *Geology*, 36;207-210, doi:
939   10.1130/G24270A.1

940 Qayyum M, R. A. Lawrence and A. R. Niem (1997), Molasse-Delta-Flysch continuum of the
941   Himalayan orogeny and closure of the Paleogene Katawaz remnant ocean, Pakistan, *Int.*
942   *Geol. Rev.*, *39*, 861–875.

943 Quittmeyer, R. C. and A. L. Kafka (1984), Constraints on plate motions in southern Pakistan
944   and the northern Arabian Sea from the focal mechanisms of small earthquakes, *J. Geophys.*
945   *Res.*, *89*, 2444-2458.

946 Rahe, B., D. Ferrill and A. Morris (1998), Physical analog modeling of pull-apart basin
947   evolution, *Tectonophysics*, *285*, 21–40.

948 Rangin C. and X. Le Pichon, Strain localization in the Sea of Marmara: Propagation of the
949   North Anatolian Fault in a now inactive pull-apart, *Tectonics*, *23*, TC2014,
950   doi:10.1029/2002TC001437, 2004

951 Reilinger R., et al. (2006), GPS constraints on continental deformation in the Africa – Arabia
952   – Eurasia continental collision zone and implications for the dynamics of plate interactions,
953   *J. Geophys. Res.*, *111*, B05411, doi:10.1029/2005JB004051.

954 Royer J.Y., A.K. Chaubey, J. Dyment, G.C. Bhattacharya, K. Srinivas, V. Yateesh and T.
955   Ramprasad (2002), Paelogene plate tectonic evolution of the Arabian and Eastern Somali
956   basins, in *The Tectonic and Climatic Evolution of the Arabian Sea Region*, edited by P.
957   Clift, D. Kroon, C. Gaedicke and J. Craig, *Geol. Soc. Spec. Publ.*, *195*, 7-23.

958 Schattner, U. and R. Weinberger (2008), A mid-Pleistocene deformation transition in the Hula
959   basin, northern Israel: Implications for the tectonic evolution of the Dead Sea Fault,
960   *Geochem. Geophys. Geosyst.*, 9, Q07009, doi:10.1029/2007GC001937.

961 Schattner, U. (2010), What triggered the early-to-mid Pleistocene tectonic transition across
962   the entire eastern Meditterranean? *Earth Planet. Sci. Lett.*, *289*, 539-548.

963 Schlische, R. W., M. O. Withjack, and G. Eisenstadt (2002), An experimental study of the
964   secondary deformation produced by oblique slip normal faulting, *AAPG Bull.*, *86(5),* 885-
965   906.

966 Seeber, L., C. Sorlien, M. Steckler, and M.-H. Cormier (2010), Continental transform basins:
967   Why are they asymmetric?, *Eos Trans. AGU, 91*(4), 29–30.

968 Shipboard Scientific Party, Site 222 (1974), in *DSDP Init. Repts*, leg 23, edited by R.B.
969   Whitmarsh, O.E. Weser and D.A. Ross, doi:10.2973/dsdp.proc.23.106.

970 Shipboard Scientific Party (1989), site 731 , in *Proc. ODP, Init. Repts., leg 117,* edited by
971   Prell, W.L., N. Niitsuma et al., College Station, TX (Ocean Drilling Program), 585-652.

972 Smit J., J. P Brun, S. Cloetingh and Z. Ben-Avraham (2008), Pull-apart basin formation and
973   development in narrow transform zones with application to the Dead Sea Basin, *Tectonics*,
974   *27*, TC6018, doi:10.1029/2007TC002119.

975 Sylvester, A. G. (1988), Strike-slip faults, *Geol. Soc. Am. Bull.*, *100*, 1666–1703.

976 Ten Brink, U. S. and Z. Ben-Avraham (1989), The anatomy of a pull-apart basin: seismic
977   reflection observations of the Dead Sea, *Tectonics*, *8*, 333-350.

978 Ten Brink, U. S. and M. Rybakov (1999), Anatomy of the Dead Sea transform; does it reflect
979   continuous changes in plate motion? *Geology*, *27*, 887-890.

980 Wakabayashi, J., J. V. Hengesh and T. L. Sawyer (2004), Four-dimensional transform fault
981   processes: progressive evolution of step-overs and bends, *Tectonophysics*, *392*, 279–301.

982 Wakabayashi, J. (2007), Stepovers that migrate with respect to affected deposits: field
983   characteristics and speculation on some details of their evolution, in *Tectonics of Strike-*
984   *Slip Restraining and Releasing Bends*, edited by W.D. Cunningham and Paul Mann, *Geol.*
985   *Soc. Spec. Publ*, *290*, 169–188.

986 Weedon, G.P. and I.N. McCave (1991), Mud turbidites from the Oligocene and Miocene
987   Indus Fan at sites 722 and 731 on the Owen Ridge, in *ODP Proc. Scientific results, leg*
988   *116,* edited by Prell, W.L., N. Niitsuma, K. Emeis et al., College Station, Texas, p. 215–
989   220.

990 Weissel, J.K., V. A. Childers and G. D. Karner (1992), Extensional and Compressional
991   Deformation of the Lithosphere in the Light of ODP Drilling in the Indian Ocean.
992   Synthesis of Results from Scientific Drilling in the Indian Ocean, Geophysical
993   Monography 70, American Geophysical Union.

994   Wesnousky, S. G. (2005), The San Andreas and Walker Lane fault systems, western North

995   America: transpression, transtension, cumulative slip and the structural evolution of a

996   major transform plate boundary, *J. Struct. Geol.*, *27*, 1505–1512

997   Whitmarsh, R.B., O. E. Weser and D. A. Ross (1974), Initial report DSDP, U.S. Government

998   Printing Office, Washington, D.C., v. 23, p. 1180.

999   Whitmarsh, R.B. (1979), The Owen Basin off the south-east margin of Arabia and the

1000   evolution of the Owen Fracture Zone, *Geophys. J. Royal Astron. Soc., 58*, 441-470.

1001   Wu, J. E., K. McClay, P. Whitehouse and T. Dooley (2010), 4D analogue modelling of

1002   transtensional pull-apart basins, *Mar. Petrol. Geol.*, *26*, 1608-1623.

1003   Zhang, P.-Z., B. C. Burchfiel, S. Chen and Q. Deng (1989), Extinction of pull-apart basins.

1004   *Geology*, *17*, 814–817.

Figure 1

a)

60°E

18°N

OFZ

OFZ

landslides

Southern
Owen
Ridge

17°N

OFZ

16°N

OFZ

Offset
12 km

15°N

Beautemps-
Beaupré
Basin

30 km

b)

60°E

OFZ

Fig. 2c

restraining
bend

inactive splay

OFZ

17°N

OFZ

10 km

c)

N   S

5000

TWT (ms)

0.8 Ma   post-folding cover
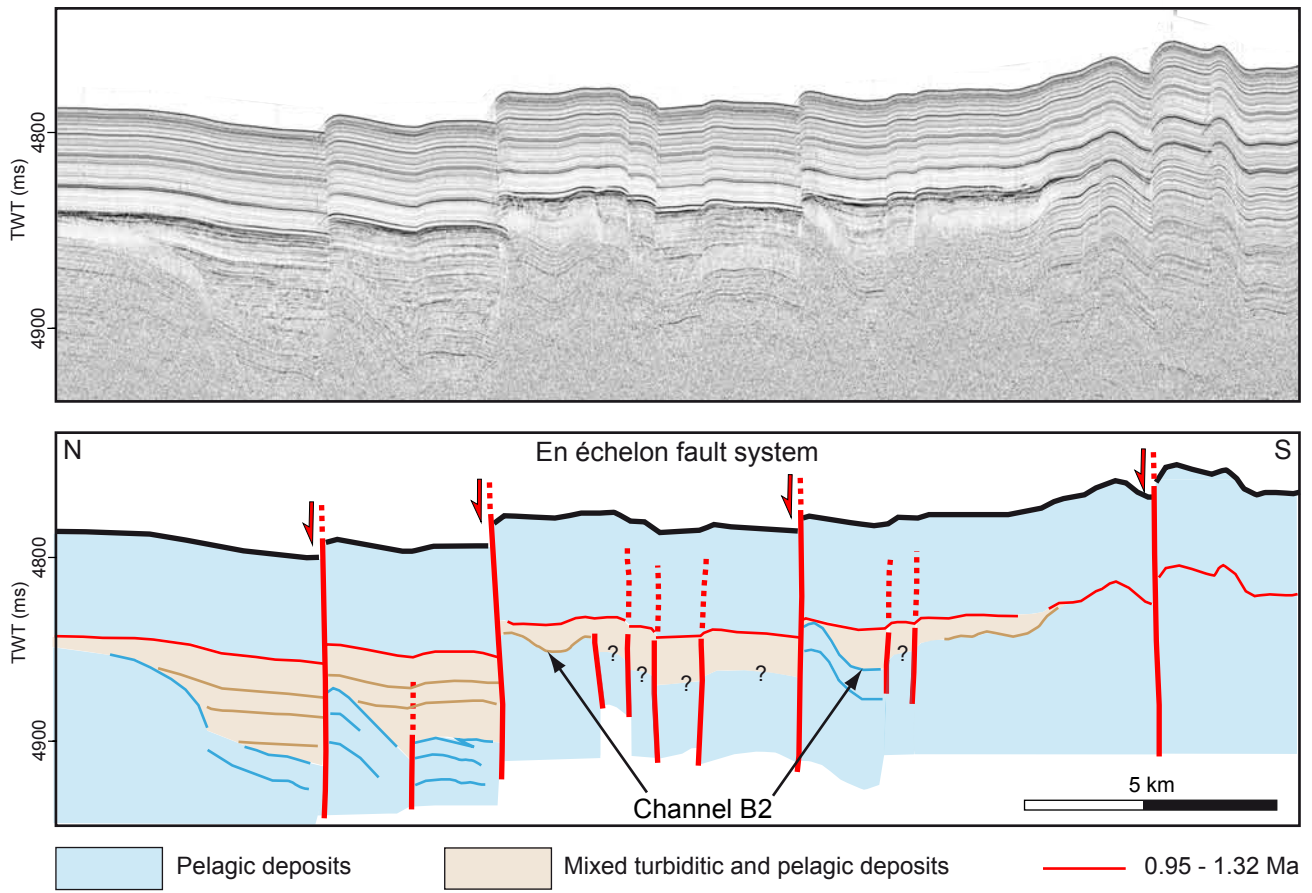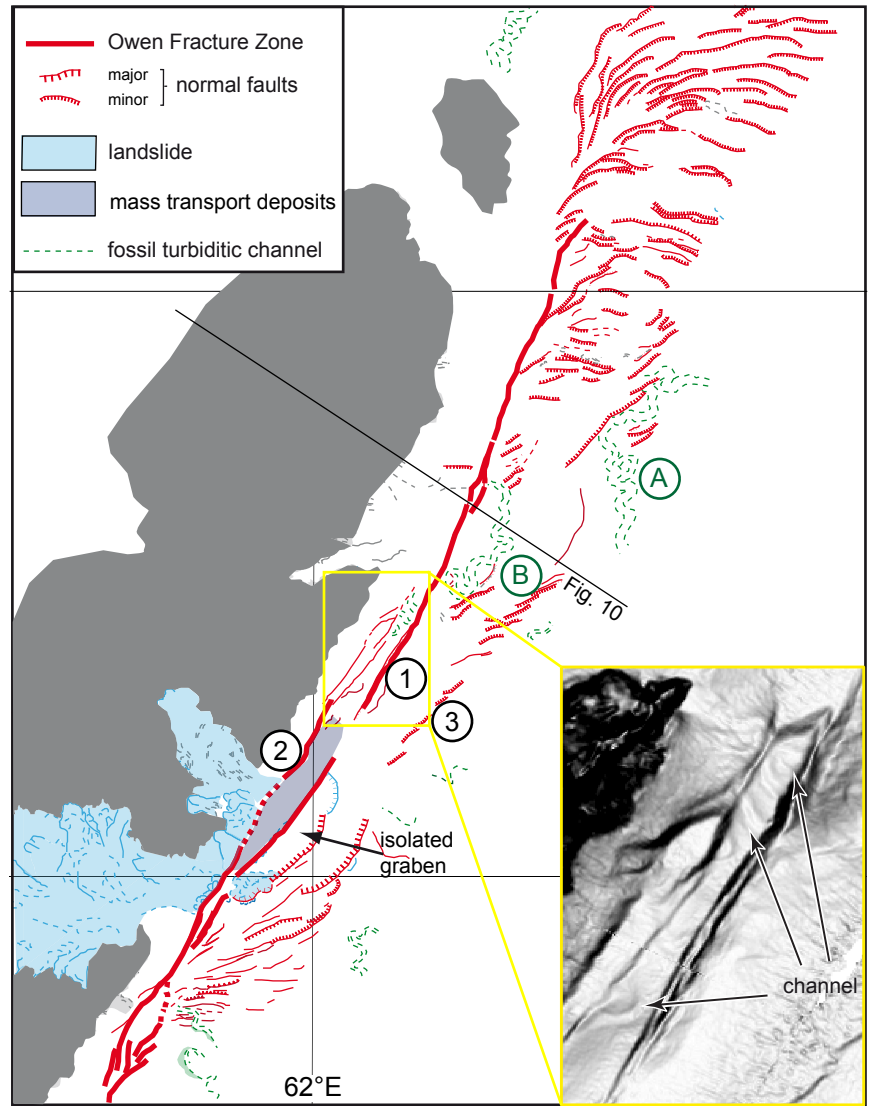
pre-folding cover

5200

mixed pelagic and
turbiditic material

5 km

fold axis

incipient fold

Figure 2

Figure 3

Figure 4

a)

N   20°N Basin   S

northern profile 2   southern profile 2

SB3   SB2   SB1

basin tilt

b)

N   Southern profile 2   S

SB2
pelagic cover

SB1
pelagic cover

paleo-
channel
B1

0.95 - 1.32 Ma

5 km

c)

N   Northern profile 2   S

SB3

transverse
growth
fault

progressively
tilted basin infill

basin tilt
α

Site of tilt
measurements

transverse fault

bench

P07a   P07b

Fig. 13

tilted
blocks

küllenberg core

5 km

Figure 5

a) Profile 7a

W — E

TWT (ms): 4800, 5000, 5200, 5400

P01, P02, P03

20°N Basin

NO DATA

paleo-channel B

Fig. c

DSDP 222

0.95 - 1.32 Ma

5 km

b) Profile 7b

W — E

TWT (ms): 4800, 5000, 5200, 5400

P02

20°N Basin

5 km

c)

TWT (ms): 4700, 4800

DSDP 222

First pelagic horizon sealing channel B3 activity

Trace of activity of channel B3

Figure 6

Figure 7

a) Profile 6

b) Profile 3

c) Profile 1

Channel C

Channel A2

Channel B3

Channel C

HARP

Channel A3

Mass transport deposit

Channel C

Channel A1

Pelagic deposits

Channel deposits

0.95 - 1.32 Myr

Channel meander

5 km
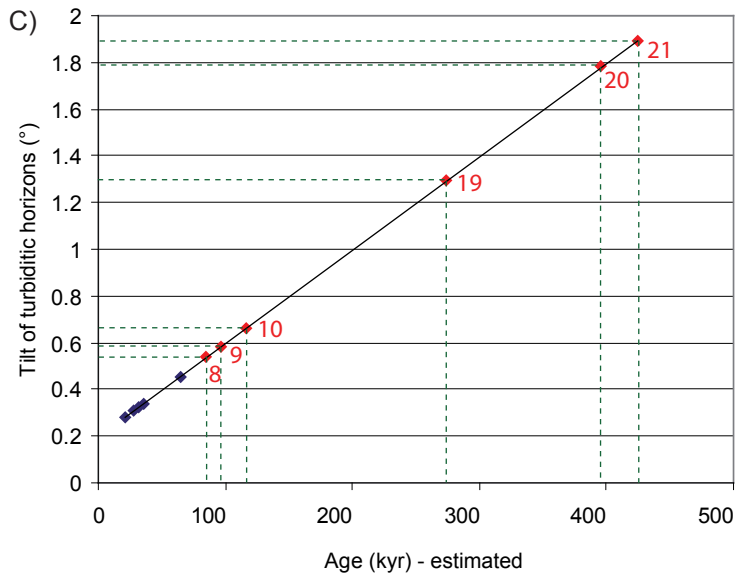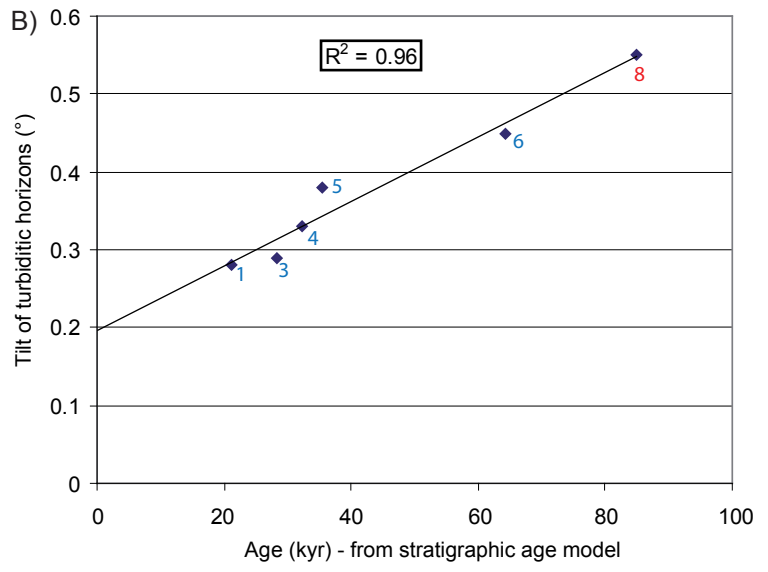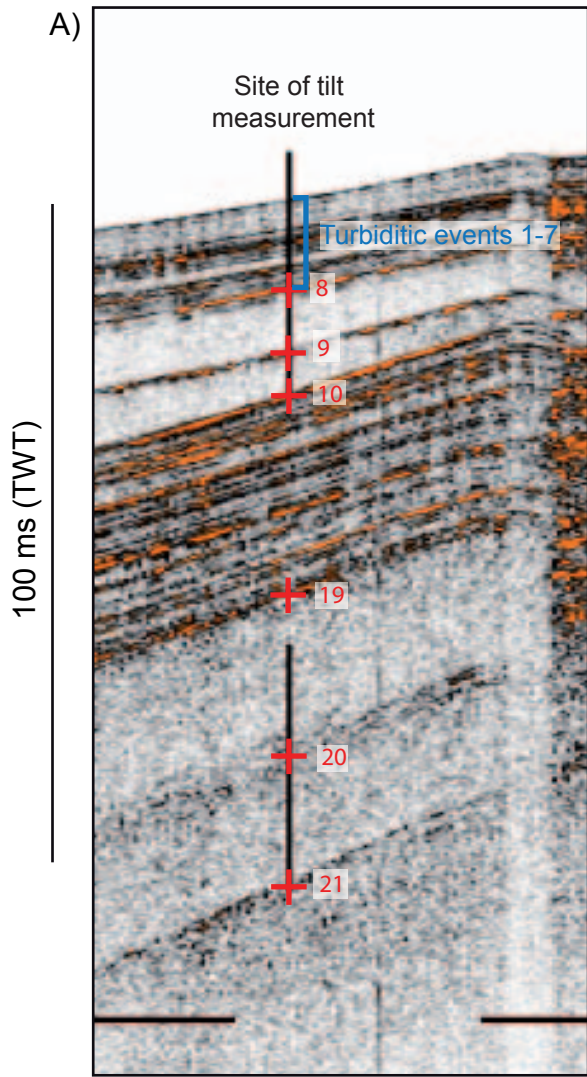
N

S

P07a

TWT (ms)

4600
4800
5000

Figure 8

Figure 9

Figure 10
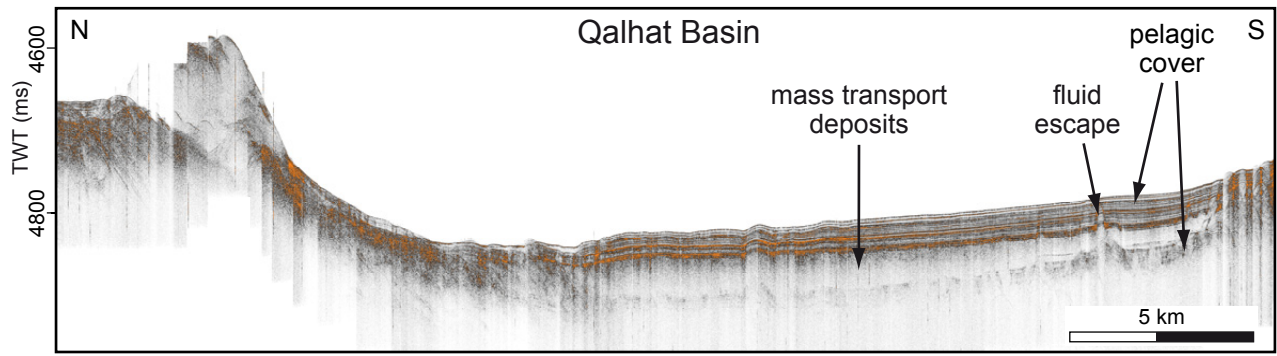
Figure 11

Figure 12

Figure 13

a) >3 Myr
62°E
22°E
Qalhat Seamount

b)
62°E
22°E
Qalhat Seamount

c) >0.8 Myr 62°E
22°E
Paleo-OFZ
Qalhat Seamount
MTD (1)

d)
62°E
22°E
migration
MTD (2)
MTD (1)

——— Owen Fracture Zone	⊤⊤⊤ normal fault	⌇⌇⌇ fossil channel
····· inferred OFZ	⌇⌇ active channel	●·●·● inferred channel trace

Figure 14

Figure 15